Robust increases in severe thunderstorm environments in response to greenhouse forcing

Noah S. Diffenbaugh[a,1], Martin Scherer[a], and Robert J. Trapp[b]

[a]Department of Environmental Earth System Science and Woods Institute for the Environment, Stanford University, Stanford, CA 94305; and [b]Department of Earth, Atmospheric, and Planetary Sciences, Purdue University, West Lafayette, IN 47907

Edited by Kerry A. Emanuel, Massachusetts Institute of Technology, Cambridge, MA, and approved August 20, 2013 (received for review April 25, 2013)

Although severe thunderstorms are one of the primary causes of catastrophic loss in the United States, their response to elevated greenhouse forcing has remained a prominent source of uncertainty for climate change impacts assessment. We find that the Coupled Model Intercomparison Project, Phase 5, global climate model ensemble indicates robust increases in the occurrence of severe thunderstorm environments over the eastern United States in response to further global warming. For spring and autumn, these robust increases emerge before mean global warming of 2 °C above the preindustrial baseline. We also find that days with high convective available potential energy (CAPE) and strong low-level wind shear increase in occurrence, suggesting an increasing likelihood of atmospheric conditions that contribute to the most severe events, including tornadoes. In contrast, whereas expected decreases in mean wind shear have been used to argue for a negative influence of global warming on severe thunderstorms, we find that decreases in shear are in fact concentrated in days with low CAPE and therefore do not decrease the total occurrence of severe environments. Further, we find that the shift toward high CAPE is most concentrated in days with low convective inhibition, increasing the occurrence of high-CAPE/low-convective inhibition days. The fact that the projected increases in severe environments are robust across a suite of climate models, emerge in response to relatively moderate global warming, and result from robust physical changes suggests that continued increases in greenhouse forcing are likely to increase severe thunderstorm occurrence, thereby increasing the risk of thunderstorm-related damage.

severe weather | CMIP5 | GCM | hazards

There now is considerable evidence that the occurrence and intensity of climate extremes have been increasing in recent decades, and that continued global warming likely will amplify these changes (1). However, the response of severe thunderstorms has remained a prominent uncertainty (e.g., ref. 1). Given the substantial damage caused by heavy rainfall, high winds, hail, and tornadoes, uncertainty about potential changes in the frequency, distribution, and intensity of severe thunderstorms poses considerable challenges for climate impacts assessment.

This uncertainty arises from at least three sources (e.g., refs. 2–5). First, there is no reliable, independent, long-term record of severe thunderstorms—and particularly tornadoes—with which to systematically analyze variability and trends (2–5). Second, theoretical arguments and climate model experiments both predict conflicting influences of the large-scale—or "environmental"—conditions that support severe thunderstorms (e.g., refs. 2–4 and 6–9). Third, a suite of processes important for the realization of individual storms in the real atmosphere has remained mostly inaccessible in climate model experiments because of deficiencies in model development and/or computational resources (e.g., refs. 3 and 10–12).

Despite these theoretical and technical challenges, both explicit and implicit modeling approaches have been used. Explicit approaches use horizontal and vertical resolutions that literally permit an explicit representation of deep convective storms and their associated characteristics (e.g., refs. 10–14). However, to date, explicit climate change experiments have been limited to short integrations of a single model (13, 14) or simulations of individual events over relatively small computational domains (12). Alternatively, implicit approaches examine the atmospheric environments that are known to support severe thunderstorm formation in the current climate (15). For example, Trapp et al. (6, 7) suggested that increasing convective available potential energy (CAPE) overcomes decreasing vertical wind shear to increase the total occurrence of severe thunderstorm environments over much of the continental United States. Although similar implicit approaches have concluded that global warming enhances conditions that support severe convection (8, 9, 16), expectations of decreasing shear continue to create uncertainty about the severe thunderstorm response (e.g., refs. 2, 3, and 8).

Here, we use the implicit approach to analyze severe thunderstorm environments in the Coupled Model Intercomparison Project, Phase 5 (CMIP5) global climate model ensemble, which offers a unique multimodel dataset of subdaily 3D atmospheric variables (17). We focus on representative concentration pathway (RCP)8.5, which covers the full range of 21st century radiative forcing and global warming spanned by the illustrative RCPs (18), thereby allowing us to probe the response to both low and high levels of forcing. We define a severe thunderstorm day using the product of vertical wind shear (over a 6-km layer; S06) and CAPE, as suggested by Brooks et al. (15) and modified by Trapp et al. (6, 7) (*Materials and Methods*). Our criteria apply to a generic severe thunderstorm environment that might result in hail, damaging "straight-line" surface winds, and/or tornadoes (6, 15). The additional existence of strong shear within the lowest atmospheric

Significance

Severe thunderstorms are one of the primary causes of catastrophic loss in the United States. However, the response of such storms to elevated greenhouse forcing has remained highly uncertain. We use an ensemble of global climate model experiments to probe the severe thunderstorm response. We find that this ensemble exhibits robust increases in the occurrence of severe thunderstorm environments over the eastern United States. In addition, the simulated changes in the atmospheric environment indicate an increase in the number of days supportive of the spectrum of convective hazards, with the suggestion of a possible increase in the number of days supportive of tornadic storms. Given current vulnerabilities, such increases imply increasing risk of thunderstorm-related damage if global warming continues.

Author contributions: N.S.D. and R.J.T. designed research; N.S.D. and M.S. performed research; M.S. contributed new reagents/analytic tools; N.S.D. and M.S. analyzed data; and N.S.D., M.S., and R.J.T. wrote the paper.

The authors declare no conflict of interest.

This article is a PNAS Direct Submission.

Freely available online through the PNAS open access option.

[1]To whom correspondence should be addressed. E-mail: diffenbaugh@stanford.edu.

This article contains supporting information online at www.pnas.org/lookup/suppl/doi:10.1073/pnas.1307758110/-/DCSupplemental.

levels (e.g., 1-km shear; S01) often is considered a key ingredient toward tornado generation (e.g., ref. 19); therefore, we consider S01 as well. We focus our analysis on the continental United States, which exhibits a globally unique confluence of peak severe thunderstorm activity (3, 15), peak density of observations (3, 15), and acute losses to severe thunderstorm events (20–22).

Results

The ensemble-mean number of days with severe thunderstorm environments (NDSEV) increases over the eastern United States in all four seasons in response to the RCP8.5 forcing pathway (Fig. 1). Winter exhibits the largest relative increase in regional mean NDSEV (exceeding 50% by the end of the 21st century; Fig. 1*A*), whereas spring exhibits the largest absolute increase (reaching 2 d per gridpoint per season; Fig. S1*N*). Spring also exhibits the most consistent response across the ensemble, with all models exhibiting positive multidecadal anomalies in regional mean NDSEV, CAPE, and surface-specific humidity after the year 2030 (Fig. 1*C* and Fig. S1 *B*, *F*, and *N*). In contrast, although summer exhibits the second largest absolute increase in regional mean NDSEV (exceeding 1 d per gridpoint per season by the end of the 21st century; Fig. S1*O*), summer also exhibits the smallest relative increase (<20%) and the least consistent response across the ensemble (Fig. 1*G*).

The spatial pattern of changes in NDSEV varies among the seasons (Fig. 1 *A*–*D*). The largest and most robust increases in the 2070–2099 period occur over the central United States in the spring season, in which widespread, highly robust increases exceed 2.4 d per season (Fig. 1*B*). Robust increases of 1.2–2.4 d per season also extend across the northern Great Plains, northern Midwest, and Northeast in spring. Widespread robust increases likewise occur over the northern Great Plains, Midwest, and Northeast in autumn, and over the Pacific Coast, Midwest, and Northeast in winter (Fig. 1*A*). The least robust changes over the United States occur during summer, with most areas exhibiting changes that are not robust (including decreases of up to −2.4 d per season over the central Great Plains), and robust increases being confined primarily over the coastal Northeast and Gulf Coast (Fig. 1*C*).

The NDSEV changes in 2070–2099 are associated with ensemble-mean increases in seasonal CAPE and ensemble-mean decreases in seasonal S06 throughout almost all areas of the continental United States in all four seasons (Fig. 2 and Fig. S1). The increases in CAPE are robust over most areas of the United States (Fig. 2 *A*–*D*) (and are associated with highly robust increases in surface-specific humidity; Fig. S2), whereas the decreases in S06 vary in robustness among the seasons and across regions (Fig. 2 *E*–*H*). The robust increases in spring NDSEV are associated with robust increases in CAPE over most areas (Fig. 2*B*). These include increases of >160 J/kg over the central and southern Great Plains, the Midwest, and the Southeast, and increases of 60–140 J/kg over the northern Great Plains and the Northeast. Spring also exhibits the smallest and least robust ensemble-mean decreases in S06 over the eastern United States (Fig. 2*F*). (The most notable exceptions occur over the Southeast, where decreases in S06 are robust and changes in NDSEV are not robust; Figs. 1*B* and 2*F*.) In contrast, summer exhibits robust decreases in S06 over much of the eastern United States (Fig. 2*G*), including over the central Great Plains, where increases in CAPE are not robust (Fig. 2*C*) and increases in surface-specific humidity are not highly robust (Fig. S2*C*). Likewise, autumn and winter exhibit the most widespread areas of highly robust decreases in S06 (Fig. 2 *E* and *H*), which tend to be associated with increases in NDSEV that are not robust (Fig. 1 *A* and *D*) despite robust increases in CAPE (Fig. 2 *A* and *D*).

The changes in CAPE and shear in the different seasons may be explained in part by changes in the vertical structure of the atmosphere (Fig. 3 and Fig. S3). For example, CMIP5 indicates negligible change in spring-season zonal wind below 8 km (Fig. 3*C*), helping explain the lack of robust change in spring-season S06 (Fig. 2*F*). In contrast, CMIP5 exhibits robust and highly robust decreases in summer-season zonal wind around 6 km (Fig. 3*F*), helping explain the robust decrease in summer-season S06 over much of the eastern United States (Fig. 2*G*). Further, although CMIP5 exhibits highly robust warming below 300 mb (~9 km) over the eastern United States in all four seasons, the vertical temperature profiles do not reveal the preferential lower-troposphere warming that would be expected to increase buoyancy (Fig. 3 *A* and *D* and Fig. S3 *A*–*D*). However, CMIP5 does exhibit highly robust increases in specific humidity that are concentrated in the lowest levels of the atmosphere (Fig. 3 *B* and *E* and Fig. S3 *E*–*H*), which would be expected to increase buoyancy. The vertical temperature and moisture profiles therefore imply that the increases in CAPE are driven by increases in low-level moisture, a result consistent with the correlation analysis of Trapp et al. (6, 7).

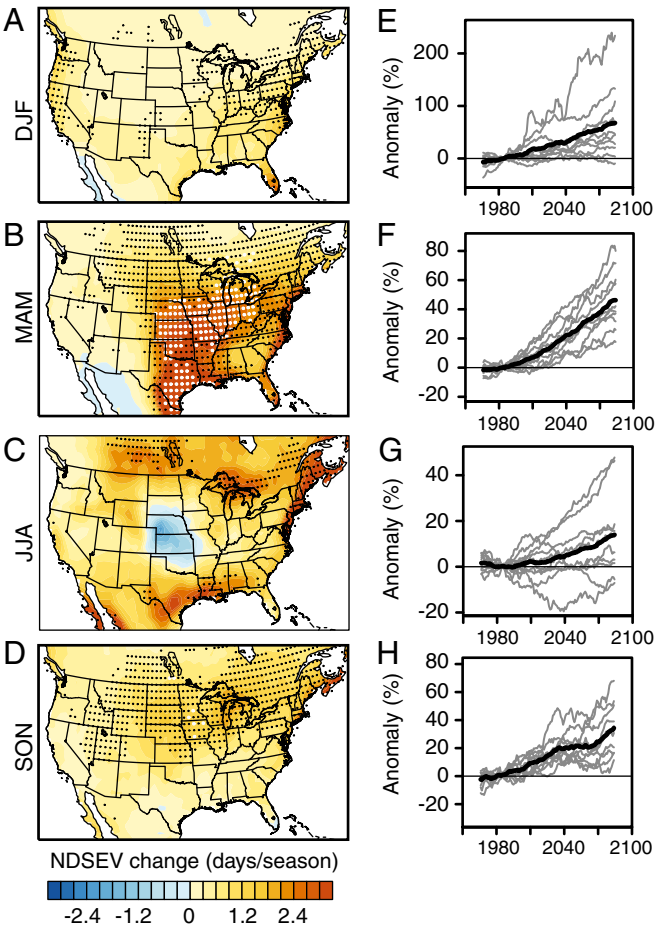

Fig. 1. Response of severe thunderstorm environments in the late 21st century period of RCP8.5 during the winter (DJF), spring (MAM), summer (JJA), and autumn (SON) seasons. (*A*–*D*) Color contours show the difference in the number of days on which severe thunderstorm environments occur (NDSEV) between the 2070–2099 period of RCP8.5 and the 1970–1999 baseline, calculated as 2070–2099 minus 1970–1999. Black (gray) dots identify areas where the ensemble signal exceeds one (two) SD(s) of the ensemble noise, which we refer to as robust (highly robust). (*E*–*H*) Each gray line shows an individual model realization. For each realization, the anomaly in the regional average NDSEV value over the eastern United States (105–67.5°W, 25–50°N; land points only) is calculated for each year in the 21st century, with the anomaly expressed as a percentage of the 1970–1999 baseline mean value. A 31-y running mean then is applied to each time series of percentage anomalies. The black line shows the mean of the individual realizations.

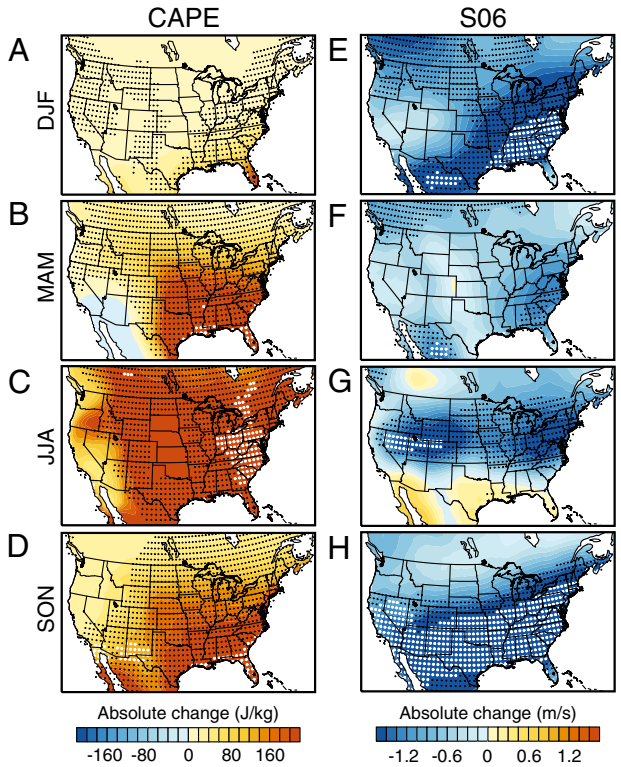

Fig. 2. Response of CAPE and wind shear in the late 21st century period of RCP8.5 during the winter (DJF), spring (MAM), summer (JJA), and autumn (SON) seasons. Differences are calculated as in Fig. 1, *Left*. (*A–D*) CAPE. (*E–H*) The magnitude of the vector difference of the horizontal wind at 6 km and the lowest model level (S06).

The influence of changing CAPE and shear on the total number of days with severe environments results from changes in the daily-scale combinations of CAPE and shear (Fig. 4). Examination of the difference in the daily-scale CAPE–shear distribution between the 2070–2099 and 1970–1999 periods reveals that the daily CAPE–S06 distribution shifts toward increasing occurrence of high CAPE in spring, summer, and autumn. As a result, the occurrence of days in which the NDSEV threshold is met increases, along with the number and fraction of severe days (SEVs) that exhibit high CAPE [e.g., CAPE >2,000 J/kg (7)] (Fig. 4 *A–D* and Fig. S4 *E*, *H*, *K*, and *N*). Likewise, the CAPE–S01 distribution also shifts toward increasing occurrence of higher CAPE, increasing the number and fraction of NDSEV that exhibit CAPE >2,000 J/kg in combination with S01 values of 10–20 m/s (Fig. 4 *A–D* and Fig. S4 *I*, *L*, and *O*). [The location of the peak decrease in the CAPE–S01 probability density function (PDF) coincides with the area of peak occurrence in the baseline distribution; Fig. S4 *F* and *O*. Note also that although the fraction of summer SEVs with high CAPE and high S01 increases, there is a greater increase in the fraction of summer SEVs with high CAPE and low S01; Fig. 4*C*.]

A key result arising from the daily CAPE–shear distributions is that the decreases in S06 are concentrated almost entirely in the low-CAPE/high-shear portion of the CAPE–S06 distribution (Fig. 4 *A–D*). Because severe environments require sufficient levels of both CAPE and shear (15), loss of high-shear days that have very low levels of CAPE essentially has no effect on NDSEV occurrence (see black curves in Fig. 4). As a result, NDSEV increases over the eastern United States in all four seasons (Fig. 1), despite decreases in mean seasonal shear (Fig. 2 *E–H* and Fig. S1 *I–L*). (Note that summer, which exhibits the least robust changes in NDSEV, does exhibit some decrease in shear at levels of CAPE that fall above the NDSEV threshold; Fig. 4*C*.)

Discussion

The CMIP5 ensemble captures many of the features of severe thunderstorm environments seen in reanalysis data over the late 20th century period. For example, CMIP5 captures the daily-scale distribution of CAPE–S06 and CAPE–S01 combinations seen in the reanalysis, including the concentration of high S06 counts on days with low CAPE (Fig. S5). In addition, the partial correlations among NDSEV, CAPE, and S06 are very similar over the eastern United States in the CMIP5 historical simulations and the reanalysis (e.g., Fig. S6), suggesting that CMIP5 captures the relative influences of CAPE and S06 on NDSEV variability. Further, the vertical gradients of temperature, moisture, and horizontal wind closely resemble those seen in the reanalysis over the eastern United States (e.g., Fig. S7).

The greatest discrepancy between the historical CMIP5 simulations and the reanalysis is the excessive occurrence of days with CAPE >4,000 J/kg in CMIP5 (Fig. S5 *F–H*). This high CAPE bias is concentrated in a subset of the models, and is particularly pronounced during the summer season (Figs. S5*G* and S8–S11). Because the convective parameterization directly or indirectly can influence how often and at what threshold CAPE is dissipated (e.g., refs. 6 and 23–26), the intermodel differences in seasonal CAPE likely are a product of the convective schemes used in the different models. The model treatment of CAPE itself also may influence the performance of the convective parameterization by influencing the atmospheric vertical structure (27). Further, the atmospheric vertical structure potentially is sensitive to the model vertical resolution, which varies considerably among the CMIP5 models (Table S1). The spread in the CAPE values among the CMIP5 models therefore highlights a need for further analysis of the complex interactions that may influence the model simulation of CAPE. However, because the changes in both CAPE and NDSEV are robust over the eastern United States (Figs. 1 *B* and *F* and 2*B*) and the physical drivers of increasing CAPE are highly robust

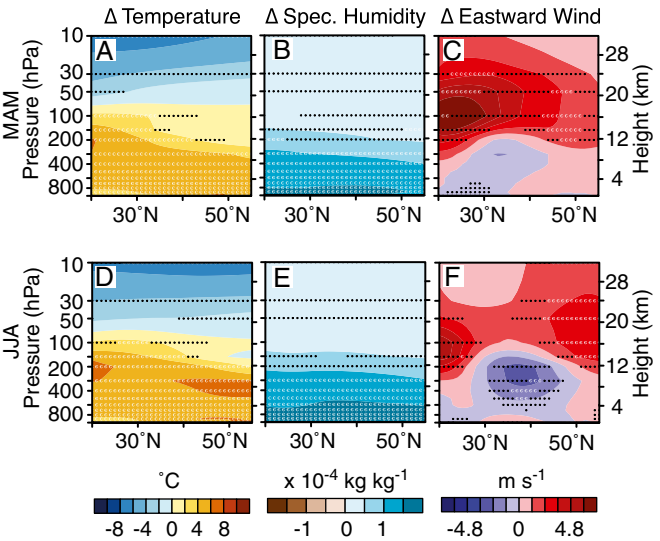

Fig. 3. Zonal mean vertical profiles in the CMIP5 ensemble for the spring (MAM) and summer (JJA) seasons. The absolute difference in ensemble-mean magnitude between the 2070–2099 and 1970–1999 periods of the CMIP5 ensemble over the eastern United States (105–67.5°W, 25–50°N) is shown. (*A* and *D*) Atmospheric temperature. (*B* and *E*) Atmospheric specific humidity. (*C* and *F*) Eastward wind. Black and gray dots identify ensemble robustness as in Fig. 1.

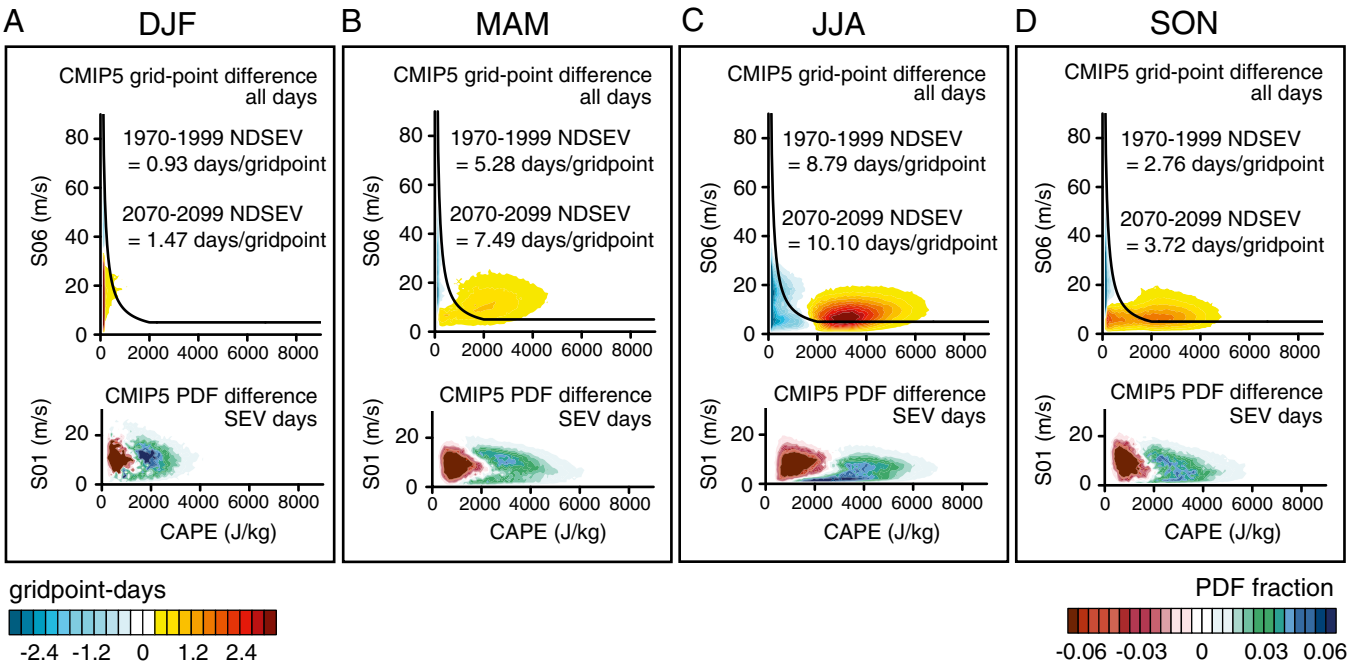

Fig. 4. Change in the frequency of occurrence of daily CAPE and shear in the winter (DJF; *A*), spring (MAM; *B*), summer (JJA; *C*), and autumn (SON; *D*) seasons in the late 21st century period of RCP8.5. Occurrences are counted for land grid points in the eastern United States (105–67.5°W, 25–50°N; land points only). The black curve shows the SEV threshold in the CAPE–S06 space. (*A–D*, *Upper*) The absolute difference in the ensemble-mean number of occurrences between the 1970–1999 and 2070–2099 periods, calculated as 2070–2099 minus 1970–1999, is shown for each season. (*A–D*, *Lower*) The absolute difference in the ensemble-mean PDF of occurrence between the 1970–1999 and 2070–2099 periods for days in which the SEV threshold is met, is shown for each season.

(Fig. 3 *A* and *B*), the increases in spring CAPE and NDSEV appear to be a robust response to increasing greenhouse forcing.

Despite the robustness of the simulated increases in NDSEV across the available CMIP5 simulations, a caveat is that severe thunderstorms occasionally occur in environments that exhibit low CAPE in combination with strong vertical shear (e.g., ref. 15). The projected decreases in shear on low-CAPE days (Fig. 4) therefore still might result in some decreases in severe thunderstorm occurrence, which in turn might offset some of the increases in high-CAPE/high-shear environments. Conversely, severe environments sometimes fail to produce severe thunderstorms. This is particularly true if high-CAPE/high-shear conditions occur when convective inhibition (CIN) also is high (e.g., ref. 28). However, the increases in occurrence of high CAPE are greatest at lower values of CIN in all four seasons (Fig. 5). As a result, the number and fraction of severe days that exhibit CAPE >2,000 J/kg in combination with CIN <100 J/kg (and with CIN <50 J/kg) increase in the late 21st century period of RCP8.5 (Fig. 5 and Fig. S12 *Q–T*). [It is noteworthy that 7 of the 10 general circulation models (GCMs) exhibit excessive CIN during the summer season, when the high CAPE bias is most pronounced (Table S2). In addition, the individual GCMs that exhibit the most consistent agreement with the reanalysis for simulated CIN (GFDL-CM3 and GFDL-ESM2M; Table S2) also exhibit the most consistent agreement for simulated CAPE (Table S2 and Figs. S8–S11 *M* and *N*) and simulated NDSEV (Figs. S8–S11 *R* and *S*).]

Another important caveat is that CAPE, shear, and CIN are implicit indicators of the atmospheric environment in which severe thunderstorms tend to occur (6, 7). Even given the insights now available from CMIP5, there are important meso- and synoptic-scale processes, especially those that aid convection initiation, that are not explicitly captured by these indicators. In particular, errors in the simulation of the atmospheric evolution may cause errors in conditions that are critical for the realization of severe storms (e.g., ref. 10). In addition, initiation of severe convection is not always well represented, even in convection-permitting models (e.g., ref. 29), highlighting the importance of improved understanding of the processes that lead to initiation of severe storms within the large-scale atmospheric environment. Likewise, S06 and S01 do not capture the important effects of hodograph curvature on convective mode and tornadogenesis. Further development of explicit approaches that permit convection in the atmosphere (e.g., refs. 10–14)—and potentially resolve individual storm dynamics (e.g., refs. 30 and 31)—will help improve understanding of the response of storm-scale processes to increasing greenhouse forcing. However, technical and computational barriers must be overcome to generate the multidecadal explicit integrations necessary to conclusively determine the likelihood of changes in the frequency, distribution, and intensity of severe thunderstorms at different levels of global warming (e.g., refs. 2, 3, and 11).

Conclusions

In addition to identifying robust increases in severe days across the CMIP5 ensemble, our analyses provide at least four key results for understanding the severe thunderstorm response to global warming. The first is that global warming results in a shift in the daily-scale CAPE/shear distribution toward a higher fraction of severe days that have high CAPE and strong low-level shear, with the increases in high CAPE being most concentrated in days with low convective inhibition. Our interpretation is of an increase in the number of days supportive of the spectrum of convective hazards (15), with the suggestion of a possible increase in the number of days supportive of tornadic storms (19).

The second key result is that increases in CAPE are robust across CMIP5, whereas decreases in S06 are concentrated mostly in days with low CAPE. Although previous work suggests that further global warming should cause increases in CAPE and decreases in shear (e.g., refs. 2–4, 6, and 7), a systematic quantification of the model agreement in the two responses previously was not possible (e.g., ref. 10), and the daily distributions of the

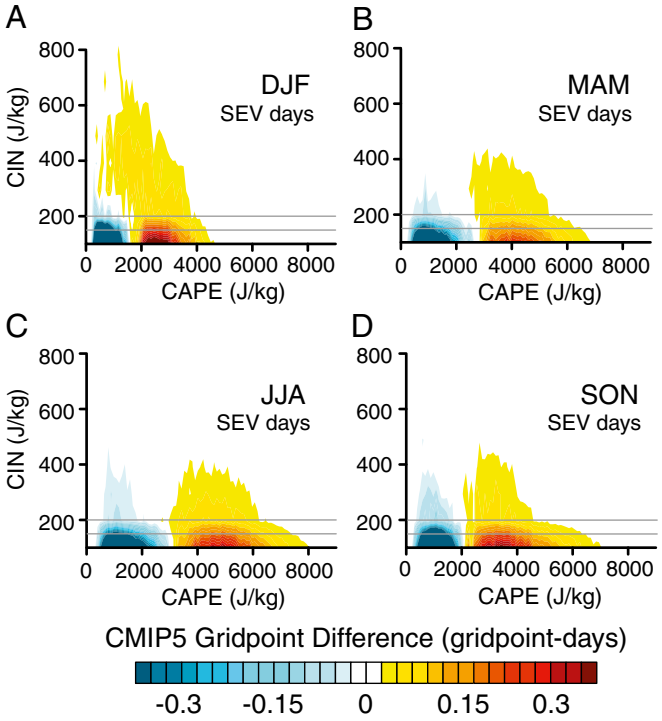

Fig. 5. Change in the frequency of occurrence of daily CAPE and CIN in the winter (DJF; *A*), spring (MAM; *B*), summer (JJA; *C*), and autumn (SON; *D*) seasons in the late 21st century period of RCP8.5. Occurrences are counted for land grid points in the eastern United States (105–67.5°W, 25–50°N; land points only) for days in which the SEV threshold is met. The absolute difference in the ensemble-mean number of occurrences between the 1970–1999 and 2070–2099 periods, calculated as 2070–2099 minus 1970–1999, is shown for each season. CIN is expressed as the absolute magnitude of the most negative accumulated buoyant energy below the LFC, yielding positive values in units of joules per kilogram. The gray lines denote the levels at which CIN equals 200 J/kg and 100 J/kg, respectively.

two responses had not been explored. The robustness and daily distributions of the CAPE and shear responses strengthen the conclusion that increases in CAPE likely lead to increases in the occurrence of severe thunderstorm environments, despite theoretically consistent decreases in shear.

The third key result is that the increases in spring and autumn CAPE and NDSEV emerge in all models before the mid-21st century in RCP8.5. Quantification of uncertainty in the transient response has been limited by the lack of transient realizations of multiple models in the same transient forcing pathway (6, 7, 12). The emergence of persistent positive regional-mean multidecadal CAPE and NDSEV anomalies across the ensemble during the midcentury of RCP8.5 suggests that lower emissions pathways also might increase the occurrence of severe thunderstorm environments over the eastern United States, including pathways that limit global warming to 2 °C above the preindustrial baseline (18).

The fourth key result is that the increases in tropospheric moisture are highly robust and concentrated in the low levels of the atmosphere. Although projected changes in CAPE and low-level humidity have been correlated in single-model experiments (6, 7), the multimodel changes in the tropospheric temperature and moisture profiles physically identify increasing low-level humidity as the primary cause of increasing CAPE, which in turn is the primary cause of increasing NDSEV.

Given the substantial damage from severe thunderstorms in the current climate, uncertainty about the response of such storms to global warming has created an important barrier to climate change impacts assessment (1). Our results indicate that continued global warming might cause substantial increases in the occurrence of the atmospheric environments associated with severe thunderstorms, because the implied reduction in vertical wind shear may not be as important as previously thought. These increases include regions where severe thunderstorms currently are most common, and regions where severe thunderstorms currently are less common but where substantial assets are exposed (3, 6, 15). Although important uncertainties about storm-scale processes still exist, the fact that the projected increases in severe environments are robust across a suite of climate models, emerge in response to relatively moderate global warming, and result from robust physical changes suggests that continued increases in greenhouse forcing are likely to increase severe thunderstorm occurrence, thereby increasing the risk of thunderstorm-related damage.

Materials and Methods

Severe Thunderstorm Environments. We quantify the occurrence of severe thunderstorm environments following the method of Trapp et al. (6, 7), who applied the empirical relationships of Brooks et al. (15). As in Trapp et al. (6, 7), we define an SEV to have occurred when (*i*) the product of S06 (the magnitude of the vector difference of the horizontal wind at 6 km and the lowest model level) and CAPE exceeds 10,000, (*ii*) CAPE exceeds 100 J/kg, (*iii*) S06 exceeds 5 m/s, and (*iv*) the horizontal wind at 6 km exceeds the wind at the lowest model level. In addition, we follow Trapp et al. (7) in also requiring that the horizontal winds at 6 km and at the surface exceed 5 m/s. Following Trapp et al. (6, 7), we calculate SEV on each day during the local afternoon, which corresponds to the typical time of maximum CAPE (6). As in Trapp et al. (6), we sum the number of days that meet the SEV criteria (NDSEV) across all days within a season.

The SEV criteria do not single out a particular convective hazard but, rather, apply to a generic severe thunderstorm environment, which might support the formation of hail, damaging straight-line surface winds, and/or tornadoes (6, 15). Unambiguous identification of a tornado-only environment is difficult because, for example, tornado-generating storms often generate large hail. However, the additional existence of strong vertical wind shear within the lowest atmospheric levels (e.g., S01, the magnitude of the vector difference of the horizontal wind at 1 km and the lowest model level) often is considered a key ingredient toward tornado generation (e.g., ref. 19); thus, we consider S01 as well.

Climate Model Ensemble. We analyze output from global climate models archived in CMIP5 (17). The CMIP5 ensemble consists of multiple GCMs for which a coordinated set of experiments have been run by participating modeling groups from around the world. Each GCM includes coupled atmosphere, ocean, land, and sea ice components. Some GCMs also include coupled biogeochemical, atmospheric chemistry, and/or dynamic vegetation components. The atmospheric components of the CMIP5 coupled GCMs vary from 0.5° to 4° in horizontal resolution (with approximately half finer than 1.3°) (17), and from 18 to 80 levels in the vertical (32). Several physical parameterizations also vary among the models, including parameterization of cumulus convection, cloud microphysics, and the planetary boundary layer.

We analyze the CMIP5 historical and RCP8.5 simulations, using the 1970–1999 period in the CMIP5 historical simulations as our baseline. RCP8.5 implies an increase in global radiative forcing of ~8.5 W/m^2 by the late 21st century, with greenhouse gas concentrations of >1,370 CO_2-equivalent (33) and median global warming of 4.9 °C above the preindustrial (18). The 21st century period of RCP8.5 covers the full range of 21st century radiative forcing and global warming spanned by the illustrative RCPs (18). Analyzing the 2070–2099 period of RCP8.5 therefore allows us to probe the response to high levels of forcing. In addition, analyzing the time-evolution over the course of the 21st century allows us to probe the response to lower levels of forcing.

Calculation of SEV in the local afternoon of each day requires subdaily, 3D atmospheric conditions from the CMIP5 simulations. [Following Trapp et al. (6, 7), we use the model-write at 00 coordinated universal time (UTC), which is the model-write closest to the local afternoon for the United States.] Although output from more than three dozen global models has been contributed to the CMIP5 archive, the requirement of subdaily, 3D atmospheric variables for the SEV calculation substantially limits the available CMIP5 ensemble. We analyze output from one realization of each of 10 models for which the necessary subdaily, 3D fields are available (Table S1).

To conform with the empirical analysis of Brooks et al. (15), we determine CAPE using an effectively mixed parcel from the lowest 100 hPa of the

modeled atmosphere. We calculate CAPE at each grid point at 00 UTC of each day (for each model). We calculate CIN as the most negative accumulated buoyant energy below the level of free convection (LFC). As with CAPE, we calculate CIN at each grid point at 00 UTC of each day (for each model). We express CIN as the absolute magnitude of the most negative accumulated buoyant energy below the LFC, yielding positive values in units of joules per kilogram.

Following the Intergovernmental Panel on Climate Change (IPCC) (34), we measure the robustness of the ensemble response to elevated forcing as the ratio between the ensemble mean response (signal) and the SD of the response in the individual model realizations (noise). We identify areas where the ensemble signal exceeds one SD of the ensemble noise (which we refer to as "robust"), and areas where the ensemble signal exceeds two SDs of the ensemble noise (which we refer to as "highly robust"). Following Giorgi (35) and Diffenbaugh and Scherer (36), we first interpolate the output from each CMIP5 model to a common 1° geographical grid.

We compare the results of the CMIP5 simulations over the baseline period with reanalysis data from the National Centers for Environmental Prediction (NCEP) (37). For these comparisons, we calculate all SEV metrics from the 6-hourly 3D NCEP variables, as in the CMIP5 calculations.

ACKNOWLEDGMENTS. We thank three anonymous reviewers and the editor for insightful and constructive comments. We acknowledge the World Climate Research Programme's Working Group on Coupled Modelling, which is responsible for CMIP, and we thank the climate modeling groups (listed in Table S1) for producing and making available their model output. For CMIP, the US Department of Energy's Program for Climate Model Diagnosis and Intercomparison provided coordinating support and led development of software infrastructure in partnership with the Global Organization for Earth System Science Portals. NCEP reanalysis data were provided by the National Oceanic and Atmospheric Administration from their Web site (www.esrl.noaa.gov/psd/). Our work was supported by National Science Foundation Grants 0756624 and 0955283 and National Institutes of Health Grant 1R01AI090159-01.

1. Intergovernmental Panel on Climate Change (2012) Managing the risks of extreme events and disasters to advance climate change adaptation. *A Special Report of Working Groups I and II of the Intergovernmental Panel on Climate Change*, eds Field CB, et al. (Cambridge Univ Press, Cambridge, UK), p 592.
2. Diffenbaugh NS, Trapp RJ, Brooks HE (2008) Does global warming influence tornado activity? *Eos* 89(53):553–554.
3. Doswell CA III, Carbin GW, Brooks HE (2012) The tornadoes of spring 2011 in the USA: An historical perspective. *Weather* 67(4):88–94.
4. Brooks HE (2013) Severe thunderstorms and climate change. *Atmos Res* 123:129–138.
5. Kunkel KE, et al. (2013) Monitoring and understanding trends in extreme storms: State of knowledge. *Bull Am Meteorol Soc* 94:499–514.
6. Trapp RJ, et al. (2007) Changes in severe thunderstorm environment frequency during the 21st century caused by anthropogenically enhanced global radiative forcing. *Proc Natl Acad Sci USA* 104(50):19719–19723.
7. Trapp RJ, Diffenbaugh NS, Gluhovsky A (2009) Transient response of severe thunderstorm forcing to elevated greenhouse gas concentrations. *Geophys Res Lett* 36: L01703.
8. Del Genio AD, Yao MS, Jonas J (2007) Will moist convection be stronger in a warmer climate? *Geophys Res Lett* 34:L16703.
9. Van Klooster SL, Roebber PJ (2009) Surface-based convective potential in the contiguous United States in a business-as-usual future climate. *J Clim* 22(12):3317–3330.
10. Trapp RJ, Halvorson BA, Diffenbaugh NS (2007) Telescoping, multi-model approaches to evaluate extreme convective weather under future climates. *J Geophys Res* 112(D20):D20109.
11. Trapp RJ, Robinson ED, Baldwin ME, Diffenbaugh NS, Schwedler BJR (2011) Regional climate of hazardous convective weather through high-resolution dynamical downscaling. *Clim Dyn* 37(3-4):677–688.
12. Mahoney K, Alexander MA, Thompson G, Barsugli JJ, Scott JD (2012) Changes in hail and flood risk in high-resolution simulations over Colorado's mountains. *Nature Climate Change* 2(2):125–131.
13. Gao Y, Fu JS, Drake JB, Liu Y, Lamarque JF (2012) Projected changes of extreme weather events in the eastern United States based on a high resolution climate modeling system. *Environ Res Lett* 7(4):044025.
14. Satoh M, Iga S-i, Tomita H, Tsushima Y, Noda AT (2011) Response of upper clouds in global warming experiments obtained using a global nonhydrostatic model with explicit cloud processes. *J Clim* 25(6):2178–2191.
15. Brooks HE, Lee JW, Craven JP (2003) The spatial distribution of severe thunderstorm and tornado environments from global reanalysis data. *Atmos Res* 67-8:73–94.
16. Lee CC (2012) Utilizing synoptic climatological methods to assess the impacts of climate change on future tornado-favorable environments. *Nat Hazards* 62(2):325–343.
17. Taylor KE, Stouffer RJ, Meehl GA (2012) An overview of CMIP5 and the experiment design. *Bull Am Meteorol Soc* 93(4):485–498.
18. Rogelj J, Meinshausen M, Knutti R (2012) Global warming under old and new scenarios using IPCC climate sensitivity range estimates. *Nature Climate Change* 2: 248–253.
19. Thompson RL, Edwards R, Hart JA, Elmore KL, Markowski P (2003) Close proximity soundings within supercell environments obtained from the Rapid Update Cycle. *Weather Forecast* 18:1243–1261.
20. Munich RE (2012) *Severe Weather in North America* (Munich RE, Munich, Germany).
21. Bouwer LM (2010) Have disaster losses increased due to anthropogenic climate change? *Bull Am Meteorol Soc* 92(1):39–46.
22. Sander J, Eichner JF, Faust E, Steuer M Rising variability in thunderstorm-related U.S. losses as a reflection of changes in large-scale thunderstorm forcing. *Weather Climate Society*, 10.1175/WCAS-D-12-00023.1.
23. Skinner CB, Diffenbaugh NS (2013) The contribution of African easterly waves to monsoon precipitation in the CMIP3 ensemble. *J Geophys Res Atmos* 118(9):3590–3609.
24. Emori S, Nozawa T, Numaguti A, Uno I (2001) Importance of cumulus parameterization for precipitation simulation over East Asia in June. *J Meteorol Soc Japan* 79(4): 939–947.
25. Straub KH, Haertel PT, Kiladis GN (2010) An analysis of convectively coupled Kelvin waves in 20 WCRP CMIP3 global coupled climate models. *J Clim* 23(11):3031–3056.
26. Zhang GJ (2009) Effects of entrainment on convective available potential energy and closure assumptions in convection parameterization. *J Geophys Res* 114(D7):D07109.
27. Neale RB, et al. (2013) The mean climate of the Community Atmosphere Model (CAM4) in forced SST and fully coupled experiments. *J Clim* 26:5150–5168.
28. Trapp RJ (2013) *Mesoscale-Convective Processes in the Atmosphere* (Cambridge Univ Press, New York), p 342.
29. Weisman ML, Davis C, Wang W, Manning KW, Klemp JB (2008) Experiences with 0–36-h explicit convective forecasts with the WRF-ARW model. *Weather Forecast* 23(3):407–437.
30. Trapp RJ, Weisman ML (2003) Low-level mesovortices within squall lines and bow echoes. Part II: Their genesis and implications. *Mon Weather Rev* 131(11):2804–2823.
31. Naylor J, Gilmore MS (2012) Environmental factors influential to the duration and intensity of tornadoes in simulated supercells. *Geophys Res Lett* 39(17):L17802.
32. Charlton-Perez AJ, et al. (2013) On the lack of stratospheric dynamical variability in low-top versions of the CMIP5 models. *J Geophys Res Atmos* 118(6):2494–2505.
33. Moss RH, et al. (2010) The next generation of scenarios for climate change research and assessment. *Nature* 463(7282):747–756.
34. Meehl GA, et al. (2007) Global climate projections. *Climate Change 2007: The Physical Science Basis. Contribution of Working Group I to the Fourth Assessment Report of the Intergovernmental Panel on Climate Change*, eds Solomon S, et al. (Cambridge Univ Press, Cambridge, UK).
35. Giorgi F (2006) Climate change hot-spots. *Geophys Res Lett* 33(8):L08707.
36. Diffenbaugh NS, Scherer M (2011) Observational and model evidence of global emergence of permanent, unprecedented heat in the 20(th) and 21(st) centuries. *Clim Change* 107(3-4):615–624.
37. Kalnay E, et al. (1996) The NCEP/NCAR 40-year reanalysis project. *Bull Am Meteorol Soc* 77(3):437–471.